Soft Matter

RSC Publishing

PAPER

View Article Online
View Journal | View Issue

Cite this: *Soft Matter*, 2013, **9**, 2730

Magnetic resonance imaging of the rheology of ionic liquid colloidal suspensions†

Jan Novak and Melanie M. Britton*

The rheology, and underpinning colloidal interactions, of ionic liquid (IL) dispersions of colloidal silica have been investigated using bulk rheological measurements with magnetic resonance (MR) velocity and relaxation measurements. Two ionic liquids were investigated: tetradecyl(trihexyl)phosphonium bistriflamide ($[P_{6,6,6,14}][NTf_2]$) and 1-butyl-methylimidizolium tetrafluoroborate ($[C_4mim][BF_4]$), in the absence and presence of hydrophilic silica nanoparticles (Aerosil 200). Bulk rheology was probed using measurements of shear stress and viscosity as a function of shear rate in a cone-and-plate rheometer. Local rheology was probed using MR velocity imaging of flow in Couette and cone-and-plate cells. Velocity profiles were extracted from the Couette measurements and fitted using a power-law model. Newtonian rheology was observed for both ILs in the absence of dispersed silica. For the dispersion of 15% silica in $[C_4mim][BF_4]$, bulk rheology and MR velocity imaging measurements showed Newtonian behaviour at low shear rates (<10 s^{-1}) and shear-thickening behaviour at higher shear rates (>10 s^{-1}). For the dispersion of 5% silica in $[P_{6,6,6,14}][NTf_2]$, more complex rheology was observed in the flow curve, which was suggestive of shear-banding. This was investigated further using the MR velocity profiles in a Couette cell and velocity images in a cone-and-plate cell, which both showed the coexistence of regions of sheared and unsheared fluid. The sheared fluid was found to be highly shear-thinning and close inspection of the flow profile at the interface between sheared and unsheared fluid suggested that the behaviour was shear-banding rather than shear-localisation. This was further confirmed by the velocity images in the cone-and-plate rheometer, which showed sheared and unsheared fluid in a uniform shear stress environment.

Received 18th October 2012
Accepted 16th January 2013

DOI: 10.1039/c3sm27409h

www.rsc.org/softmatter

1 Introduction

Over the last 20 years or so, ionic liquids (ILs) have received significant interest as solvents for synthesis and catalysis,[1] electroytes,[2] lubricants[3,4] and media for the formation and stabilisation of nanoparticles.[5–8] Their physical, chemical and electrochemical properties make them suitable for an enormous range of applications and it is their ability to enhance colloidal stability[7] and prevent aggregation of nanometre-sized particles that makes them useful as media for nanoparticle synthesis,[9,10] solidified electrolytes[8] and magnetorheological fluids.[11,12] While there has been considerable investigation towards the application of ILs as dispersion media for colloidal particles, there are relatively few studies investigating the fundamental science[6,7,13–15] underpinning the molecular processes involved. Recently, Ueno *et al.*[5–7,16] researched colloidal stabilisation, using silica nanoparticles in room temperature ILs (RTILs), investigating their ionic transport, microstructure and rheology. The addition of colloidal particles to fluids, can lead to the formation of gels or produce other viscoelastic behaviour, such as shear-thinning, shear-thickening or thixotropy.[6,17] While, rheological studies of these systems allow their viscoelastic properties to be characterised, they can also provide further insight into the colloidal interactions present.[6,7,17] In their recent paper,[6] Ueno *et al.* reported rheological measurements of suspensions of hydrophobic and hydrophilic silica nanoparticles in a range of RTILs. They observed both shear-thickening and shear-thinning behaviour and found that the rheology of the colloidal silica-RTIL dispersions was strongly affected by the ionic structure of the ILs, as well as the surface-chemistry of the silica particles. These rheological responses were then associated with differences in the internal structure of the suspensions, with shear-thinning and colloidal gelation being associated with flocculated systems and shear-thickening associated with stable suspensions.[7] Thus, the rheology of IL suspensions can be tailored by choosing hydrophobic or hydrophilic ILs or silica, as certain hydrophilic ILs exhibit shear-thickening behaviour over a range of hydrophilic silica concentrations and hydrophobic ILs show shear-thinning behaviour over a range of silica concentrations.[5,6]

While rheological measurements provide an opportunity to test how the surface chemistry of the silica particles or

School of Chemistry, University of Birmingham, Edgbaston, Birmingham, B15 2TT, UK. E-mail: m.m.britton@bham.ac.uk

† Electronic supplementary information (ESI) available. See DOI: 10.1039/c3sm27409h

composition of the ionic liquid affect the viscoelastic properties of the colloidal dispersion, they are not able to directly relate complex fluid rheology to microscopic structure and dynamics. Also, rheological experiments, which measure changes in shear stress and viscosity as a function of shear rate, assume spatial uniformity of fluid behaviour. However, this assumption breaks down for many complex fluids, even under the conditions of uniform stress.[18–21] This is particularly the case for fluids which exhibit shear-localisation[22] or shear-banding,[23,24] which has been observed in wormlike micelle solutions,[20] as well as colloidal suspensions.[22,25,26] In this paper we investigate the localised rheology of colloidal suspensions of hydrophilic silica particles in two room-temperature ILs, tetradecyl(trihexyl)phosphonium bistriflamide ($[P_{6,6,6,14}][NTf_2]$) and 1-butyl-methylimidizolium tetrafluoroborate ($[C_4mim][BF_4]$), using magnetic resonance (MR) velocity imaging, and compare with macroscopic rheological measurements. The ILs investigated were either hydrophilic ($[C_4mim][BF_4]$) or hydrophobic ($[P_{6,6,6,14}][NTf_2]$), and exhibited shear-thickening or shear-thinning behaviour, respectively, when hydrophilic silica was suspended in them.

1.1 Magnetic resonance velocity imaging

Magnetic resonance imaging (MRI) has provided valuable and sometimes unique insight into the rheology of complex fluids such as wormlike micelles,[20] lubricating greases,[18] polymer solutions,[27,28] concentrated suspensions[22,29] and food materials[21,30] in a variety of rheometric devices.[19] Unlike conventional rheometric measurements, which produce averaged values integrated over the bulk of the sample, MR velocity measurements are able to probe the localised rheology of a sample. Using these measurements it is possible to observe shear-banding and shear-localisation.[20,22–24]

MR velocity images are typically acquired using a pulsed gradient spin echo (PGSE) imaging sequence,[31] combining a 2-dimensional imaging sequence with two narrow magnetic field gradient pulses of duration δ, separation Δ and strength $\boldsymbol{g}$. These PGSE gradient pulses impart phase shifts in the MR signal of spins in the sample, which arise from molecular displacement over the time scale Δ. In the case of flow, where molecular motion is coherent, a net phase shift, ϕ, is produced which is dependent on γ (the magnetogyric ratio), δ, Δ, $\boldsymbol{g}$ and the flow velocity v (eqn (1)).

$$\phi = \gamma v \boldsymbol{g} \delta \Delta \tag{1}$$

Where a series of images are acquired, with $\boldsymbol{g}$ ramped from zero to $\boldsymbol{g}_{max}$, the velocity of molecules within each pixel can be extracted using Fourier analysis of the data with respect to $\boldsymbol{q}$, where $\boldsymbol{q} = \gamma \boldsymbol{g} \delta / 2\pi$. Fourier transformation produces a probability distribution function (propagator) for displacements over the time Δ for each pixel in the image.[32,33] The velocity is given by the offset of the propagator. Further details on these methods can be found elsewhere.[31]

By acquiring velocity images for fluid sheared in a Couette cell, it is possible, using a power law model, to determine the rheology of the fluid by extracting a velocity profile through the annulus and fitting it to eqn (2). This equation is an analytical expression for the azimuthal component of the velocity field, v_ϕ, of a power-law fluid at position $\boldsymbol{r}$ in a cylindrical Couette cell, where the outer cylinder, of radius r_o, is stationary and the inner cylinder, of radius r_i, rotating at an angular speed of Ω, with $K = r_i/r_o$, $R = r/r_o$ and n is the power law exponent.[34]

$$v_\phi = \Omega r_i \frac{R(1 - R^{-2/n})}{K(1 - K^{-2/n})} \tag{2}$$

By fitting the data to eqn (2), it is possible to determine whether the fluid is Newtonian in behaviour, where $n = 1$, shear-thinning ($n < 1$) or shear-thickening ($n > 1$). In addition to determining the power law exponent, other rheological behaviour, such as yield stress, shear-localisation or shear-banding can also be observed from the velocity profiles of fluid in the Couette cell.[21,35] Other rheometric devices, such as the cone-and-plate rheometer, which is able to provide a uniform stress environment, have also been investigated using magnetic resonance velocity measurements and have been used to investigate shear-localisation[29] and shear-banding[20] behaviour.

1.2 Shear-banding and shear-localisation

Shear-banding is a phenomenon where fluid coexists in two phases at equal stress but different shear rates.[24,36,37] Shear-banding can be observed in plots of shear stress (σ) *vs.* shear rate ($\dot{\gamma}$), known as flow curves, which exhibit a plateau in the shear stress, above a critical shear rate ($\dot{\gamma}_c$). In the region of this stress plateau, the apparent shear rate ($\dot{\gamma}$) is a sum of the relative proportions of the lower ($\dot{\gamma}_l$) and higher ($\dot{\gamma}_h$) shear rate phases:

$$\dot{\gamma} = \phi_l \dot{\gamma}_l + \phi_h \dot{\gamma}_h \tag{3}$$

where ϕ_l and ϕ_h are the relative proportions of the lower and higher shear rate. In the case of shear-banding of wormlike micelles in a cone–plate rheometer, shear bands take the form of a high-shear band in the middle of the gap with low-shear bands on either side. As the apparent shear rate increases above $\dot{\gamma}_c$, the width of the high-shear band, and hence ϕ_h, increases, while $\dot{\gamma}_h$ and $\dot{\gamma}_l$ remain relatively constant.[20]

The phenomenon of shear-localisation has similar features to shear-banding, however it is fundamentally different. Shear-localisation describes a situation where there is a coexistence of static and flowing material[22] and found in yield stress materials where the shear stress is not uniform, such as that found in pipe of Couette flow. In shear-localisation, a continuous transition in the slope of the velocity profile is observed at the interface between the sheared and unsheared regions. In shear-banding, different shear rates coexist at constant shear stress, and is found in rheometers where the shear stress is uniform such as in a cone-and-plate rheometer[23,24] and a discontinuity is observed in the velocity profile at the interface between the different shear rate regions.[25,29]

2 Experimental

2.1 Materials and chemicals

Tetradecyl(trihexyl)phosphonium bistriflamide $[P_{6,6,6,14}][NTf_2]$, (Cytec, Canada), 1-butyl-methylimidizolium tetrafluoroborate $[C_4mim][BF_4]$, (Aldrich, UK) and Aerosil 200 (Evonik, Germany)

were used as received without further purification. Aerosil 200 is fumed silica made hydrophilic by surface functionalisation with Si–OH groups. The silica particles were 12 nm in diameter and were dispersed in the ionic liquid using an overhead stirrer. Rheology and MR velocity imaging experiments were performed on the pure ILs, $[C_4mim][BF_4]$ + 15% wt Aerosil 200 and $[P_{6,6,6,14}][NTf_2]$ + 5% wt Aerosil 200.

2.2 Rheometry

Rheology measurements were conducted on a AR-G2 rheometer (TA Instruments) using a cone-and-plate geometry (60 mm diameter, 2° gap) at 298 ± 0.1 K. Steady-state flow experiments were conducted with 10 points per decade, logarithmically spaced between 0.05 and 1000 s^{-1}. Rheometry measurements of Aerosil 200 suspensions in $[C_4mim][BF_4]$ were collected over a range of concentrations from 0 to 15% wt and showed similar behaviour to that reported by Ueno *et al.*[6] Viscosity plots and flow curves are shown for 0 and 15% in this paper and for 5 and 10% in the ESI (Fig. S1†). Measurements for the $[P_{6,6,6,14}][NTf_2]$ IL were made for the neat IL and a 5% wt Aerosil 200 suspension. It was not possible to exceed a concentration of 5%, as the silica could not be suspended beyond this concentration and resulted in a biphasic material.

2.3 Magnetic resonance imaging

NMR measurements were performed on a Bruker DMX 300 spectrometer, which operates at a proton resonance frequency of 300.13 MHz. The temperature of the bore of the magnet was 289 ± 0.3 K. Experiments were performed using a 25 mm birdcage radio-frequency resonator and water-cooled, triple-axis magnetic field gradients with a maximum gradient strength of 100 G cm^{-1}. Velocity measurements were performed on fluid inside the annulus of a Couette cell consisting of a glass outer cylinder of radius (r_o) 5.7 mm and an inner cylinder with a radius (r_i) of 2.6 mm. The inner cylinder of the Couette cell was rotated inside the MRI magnet using a drive shaft, which was controlled by a stepper motor (Bruker Rheo-NMR System). Velocity images were acquired using a pulsed gradient spin echo (PGSE) imaging sequence.[21,27,32] Horizontal images of the Couette cell were acquired (Fig. 1), with a slice thickness of 3 mm, field of view of 13 mm × 13 mm and a matrix size of 128 (phase) × 64 (read) pixels, resulting in a pixel size of 0.156 mm × 0.172 mm. The resolution was limited in the read direction by the spread of chemical shifts for the proton resonances in the ILs[38,39] (2440 Hz for $[C_4mim][BF_4]$ and 600 Hz for $[P_{6,6,6,14}][NTf_2]$), so that the frequency range within a single pixel was greater than that of the chemical shift range. Velocity measurements were acquired at rotation rates of 1–4 Hz and typical PGSE parameters were $g_{max} = 0.26$–0.55 T m^{-1}, $\delta = 1$ ms and $\Delta = 10$ ms. A recovery time (T_R) of 1 s was used.

NMR velocity measurements were performed on the $[P_{6,6,6,14}][NTf_2]$ + 5% wt Aerosil system in a cone-and-plate device inside the MRI magnet, comprising a plate and cone of angle 20°, manufactured from PEEK. Fluid in the gap of the cone and plate was surrounded with a PTFE ring of inner diameter 19.5 mm. The cone was rotated in the same way as the Couette cell. Vertical images were acquired with a slice thickness of 1 mm, field of view of 20 mm (horizontal) × 18 mm (vertical) and matrix size of 64 × 256 pixels, respectively, which resulted in a pixel size of 0.313 mm (horizontally) × 0.070 mm (vertically). Velocity images were acquired at angular velocities of $\omega = 0.08$–0.32 Hz (using a stepper motor range of 1–4 Hz and a 25 : 2 gearbox), with PGSE parameters of $g_{max} = 0.26$–0.55 T m^{-1}, $\delta =$ 1 ms and $\Delta = 10$ ms. A recovery time (T_R) of 1 s was used for all experiments.

NMR relaxation maps[33] in the Couette cell, were acquired for the $[P_{6,6,6,14}][NTf_2]$ + 5% wt Aerosil system acquired with a slice thickness of 2 mm, a field of view of 1.3 × 1.3 mm and matrix size of 64 × 64 pixels. A repetition time of $T_R = 4$ s was used to ensure $T_R > 5T_1$ for all ^1H resonances in the ILs. T_1 relaxation

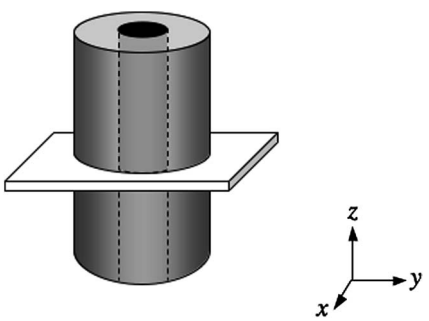

Fig. 1 Schematic diagram showing the Couette cell geometry and image orientation for the horizontal velocity images acquired.

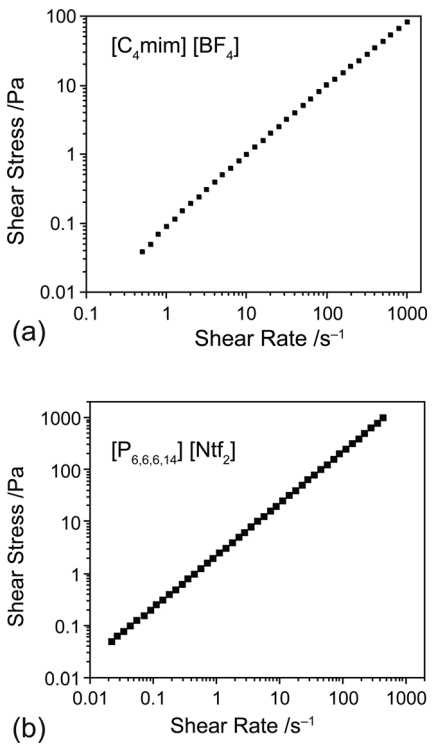

Fig. 2 Flow curves, showing shear stress as a function of shear rate, for neat $[C_4mim][BF_4]$ (a) and $[P_{6,6,6,14}][NTf_2]$ (b) ionic liquids.

maps were produced from a series of six spin echo MR images with varying T_1 inversion recovery delays from 10 to 1500 ms.

The NMR data was analysed using Prospa NMR analysis software.[40] Velocity profiles, along the centre of the Couette cell, were extracted from the horizontal images and fitted using eqn (2), to determine power law exponents.

3 Results and discussion

Flow curves for $[P_{6,6,6,14}][NTf_2]$ and $[C_4mim][BF_4]$ ILs, without colloidal silica, are shown in Fig. 2. In both ILs, Newtonian behaviour is observed. MR velocity profiles in a Couette cell for these ILs are given in Fig. 3. The velocity profiles also show Newtonian behaviour, as fitting of the MR velocity profiles to eqn (2) returns power law exponents of $n = 1$ for each plot.

A flow curve and plot of viscosity *vs.* shear-rate for a 15% suspension of hydrophilic colloidal silica (Aerosil 200) in $[C_4mim][BF_4]$ are shown in Fig. 4. In these plots, more complex rheology is observed than in the pure IL. At low shear rates ($\leq$10 s^{-1}), Newtonian behaviour is observed, where the viscosity is constant as a function of $\dot{\gamma}$. However, above a shear rate of approximately 10 s^{-1} the suspension becomes shear-thickening up to a shear rate $\dot{\gamma} > 100\ s^{-1}$, where the fluid starts to be ejected from the cone-and-plate rheometer. A transition from Newtonian to shear-thickening behaviour is also observed in the MR velocity profiles for this system (Fig. 4c). Power law exponents

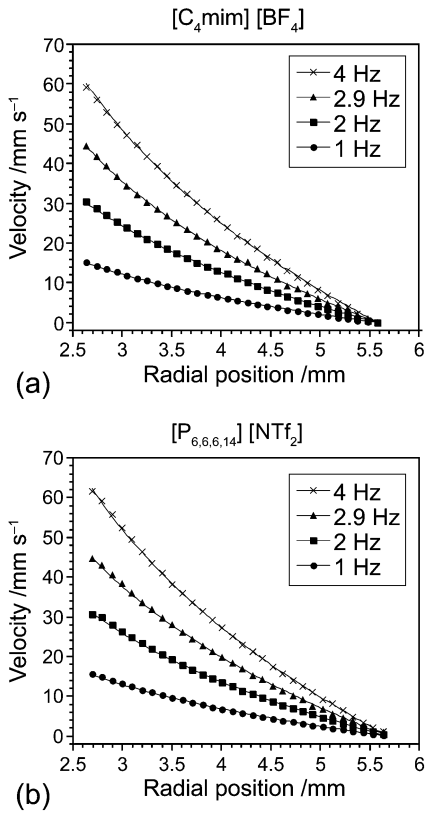

Fig. 3 Radial velocity profiles taken across the cylindrical Couette cell for neat $[C_4mim][BF_4]$ (a) and $[P_{6,6,6,14}][NTf_2]$ (b) ionic liquids at rotation rates of $\omega = 1$, 2, 2.9 and 4 Hz. The line shows the fit obtained using eqn (2), which yielded a value of $n = 1$ (Newtonian behaviour) in both cases.

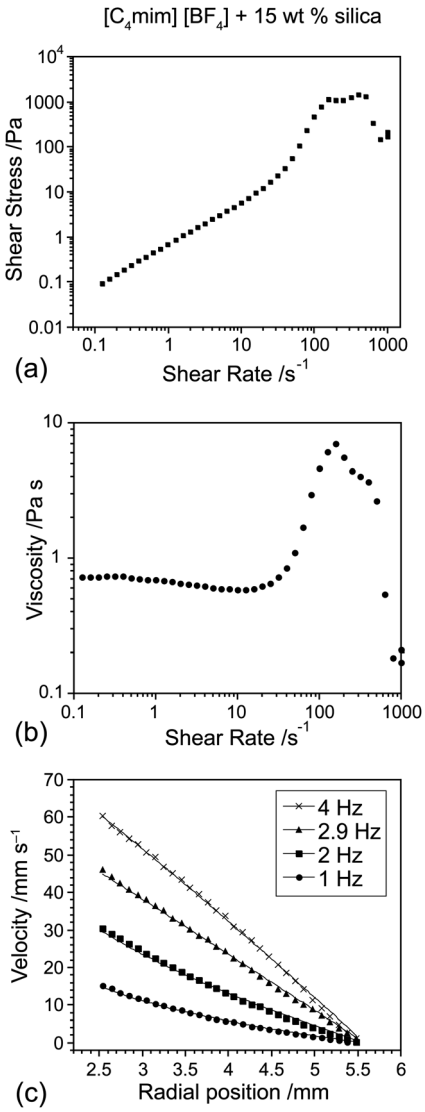

Fig. 4 Flow curve (a), plot of viscosity *vs.* shear rate (b) and radial velocity profiles in a Couette cell (c) for $[C_4mim][BF_4]$ with 15% w/w Aerosil 200. The line in (c) shows the fit obtained using eqn (2), which yielded values of $n = 1.01$ at 1 Hz, $n = 1.22$ at 2 Hz, $n = 2.04$ at 2.9 Hz and $n = 2.67$ at 4 Hz.

for this system at each rotation rate shows an increase in the shear-thickening behaviour, with values of $n = 1.01$ at 1 Hz, $n = 1.22$ at 2 Hz, $n = 2.04$ at 2.9 Hz and $n = 2.67$ at 4 Hz determined. Such a transition from Newtonian to shear-thickening behaviour has also been observed in this system by Ueno *et al.*[6] In their rheological measurements, they found these suspensions exhibited low, shear-independent viscosity at low shear rates, with a dramatic increase in viscosity at higher shear rates. They associated the Newtonian behaviour and low viscosity to the formation of a stabilised suspension and an absence of an internal silica network structure. The stabilisation of the colloidal particles is often linked to the formation of solvation layers around the particles, which is supported by the observation of hydrogen bonds between the F atoms in the $[BF_4]$ anions to surface silanol groups.[41] What leads to the increase in viscosity, as the shear rate increases, is possibly a disruption of

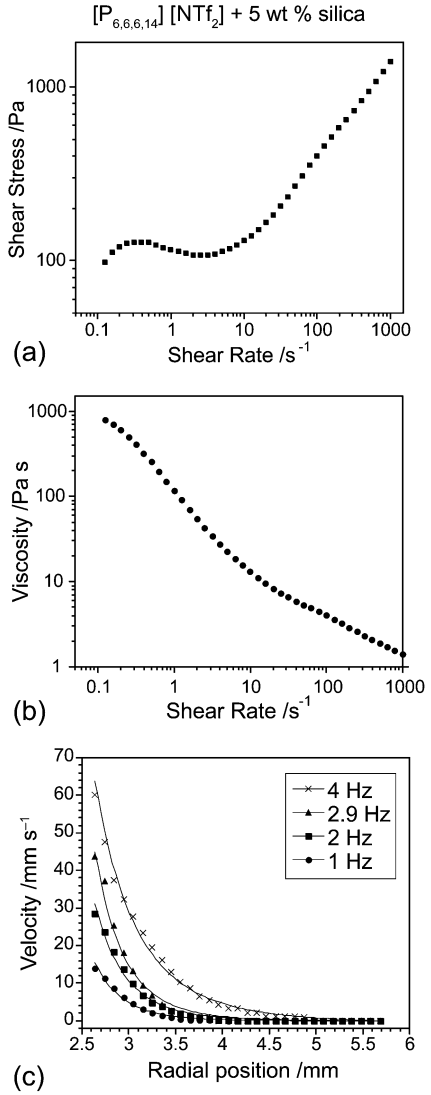

Fig. 5 Flow curve (a), plot of viscosity *vs.* shear rate (b) and radial velocity profiles in a Couette cell (c) for $[P_{6,6,6,14}][NTf_2]$ with 5% w/w Aerosil 200. The line in (c) shows the fit obtained using eqn (2), which yielded values of $n = 0.20$ at 1 Hz, $n = 0.21$ at 2 Hz, $n = 0.28$ at 2.9 Hz and $n = 0.21$ at 4 Hz.

these solvation layers, leading to a destablisation of the suspension. This shear-thickening behaviour is also seen at lower concentrations of silica (see ESI, Fig. S1† and ref. 6), however the shear-thickening is most pronounced in the 15% suspension.[6] Also, in our rheometry measurements of the 15% suspension, the onset of shear-thickening was found at a shear rate of *circa* 30 s^{-1}. This provided an opportunity to probe both Newtonian and non-Newtonian behaviour using MRI measurements in a Couette cell, where the accessible shear rates were able to cover the shear rates below and above the onset of shear-thickening behaviour (see ESI†).

The flow curve and plot of viscosity *vs.* shear-rate for a 5% suspension of hydrophilic colloidal silica (Aerosil 200) in $[P_{6,6,6,14}][NTf_2]$ (Fig. 5) also shows complex rheological behaviour. In the flow curve, the shear stress appears to almost form a plateau between shear rates 0.3 s^{-1} and 10 s^{-1}, after which the shear stress increases. This type of behaviour in the flow curve has been observed in fluids undergoing shear-banding.[37] In the corresponding viscosity plot, shear-thinning behaviour is observed, with a transition at approximately 10 s^{-1}. Shear-thinning behaviour is typically expected in concentrated systems, as is yield stress behaviour, where fluids only flow when the applied stress exceeds a critical (yield) stress value. Yield stress behaviour is associated with the disruption of a network of interactions between mesoscopic particles and these materials will flow at a rate that increases as the difference between the applied stress and yield stress increases.[29] Our findings, highlight one of the main problems with conventional rheological measurements, which is that they are integrated over the whole sample and so cannot identify or investigate localised rheology. The advantage with the MR velocity measurements, becomes apparent in systems under-going shear-banding or other shear-localisation phenomena. The MR velocity profile (Fig. 5c) is able to directly visualise the local rheology produced in this system. By fitting these velocity profiles to eqn (2), power-law exponents of $n = 0.20$ at 1 Hz, $n = 0.21$ at 2 Hz, $n = 0.28$ at 2.9 Hz and $n = 0.21$ at 4 Hz were determined, showing that the fluid in this region is highly shear-thinning.

The velocity profiles in Fig. 5c suggest that the fluid is split into two regions: one sheared, the other unsheared. As a result, the data was re-fitted to eqn (2), so that the outer radius became a fitting parameter, allowing it to move towards the boundary between sheared and unsheared regions. The resulting fits returned the following power-law exponents and r_o values: $n = 0.19$ and $r_o = 4.43$ mm at 1 Hz, $n = 0.21$ and $r_o = 4.54$ mm at 2 Hz, $n = 0.20$ and $r_o = 4.43$ mm at 2.9 Hz and $n = 0.27$ and $r_o = 5.4$ mm at 4 Hz. Fig. 6, shows the velocity profile at 2 Hz with both fits included. While, a better fit is possible by allowing r_o to move towards the interface between sheared and unsheared regions, this model is still not able to fit the velocity profile well. This region has been expanded and included in the inset plot in Fig. 6. The velocity profile at the interface suggests that the shear rate is not continuous and may suggest that rather than simple shear-localisation, where both static and flowing regions coexist, shear-banding is occurring. As is shown more clearly in

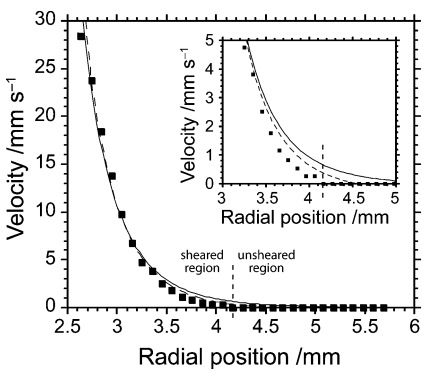

Fig. 6 Radial velocity profiles taken across the cylindrical Couette cell for $[P_{6,6,6,14}][NTf_2]$ with 5% w/w Aerosil 200 at a rotation rate of $\omega = 2$ Hz. The inset plot shows the region by the interface at an expanded scale. The solid line is the fit to eqn (2) with r_o fixed and $n = 0.21$ and the dashed line is the fit with r_o as a fitting parameter with $r_o = 4.54$ mm and $n = 0.21$.

the inset plot in Fig. 6, the velocity profile does not smoothly decrease to zero and in this region deviates from the power-law model. This has previously been suggested[22] as an indicator of shear banded flow, rather than shear-localisation. To test whether this behaviour was associated with changes in the molecular dynamics of the solvent, the system was studied using MR relaxation measurements.

In semi-dilute polyacrylamide solutions in water,[28] shear-thinning behaviour has been associated with changes in the reorganisational dynamics of the polymer molecules in the system, which was detected using T_2 MR relaxation measurements. With this in mind, we investigated whether the IL molecules in the region of shear-thinning had changes in T_1 or T_2 MR relaxation times, which might also be associated with changes in the mobility and dynamics of these molecules. T_1 and T_2 relaxation maps were produced for the $[P_{6,6,6,14}][NTf_2]$ + 5% colloidal silica system in the Couette cell, at a range of rotation rates. The azimuthal averages of the relaxation time of fluid in the annulus of the Couette cell, at $\omega = 1$ Hz, are shown in Fig. 7. While slight reductions are observed at the walls of the Couette cell, no variation is seen through the annulus, and in particular there is no difference between the sheared and unsheared regions. This could suggest that if the IL molecules are forming a solvation shell around the silica particles, as has been suggested as a mechanism for stabilising silica particles in $[C_4mim][BF_4]$ and $[C_2OHmim][NTf_2]$ ILs, then the structure and dynamics of this solvation shell is not significantly affected by the shear. However, as shear-thinning behaviour is observed for the sheared part of the suspension, it is more likely that a colloidal gel has formed,[7] where the dispersed colloidal particles are unstable and form interconnecting networks through the system. It has been observed, that in these types of systems the ionic conductivity and diffusivity is mostly unaffected by the addition of the silica particles.[7] Our relaxation measurements also appear to agree with these previous observations. Further investigation is required and in particular measurements of the behaviour of the anion are desirable, which will require ^{19}F NMR measurements.

The presence of shear-banded flow was further explored in a cone-and-plate rheometer, where the shear stress is more uniform across the sheared fluid than in a Couette cell. This system is particularly useful in distinguishing between simple shear-localisation, due to yield stress behaviour and a large variation in the shear stress of a system, and true shear-banding.[22] In Fig. 8, a series of velocity images are shown for flow of a 15% colloidal silica suspension in $[P_{6,6,6,14}][NTf_2]$ in a cone-and-plate rheometer. Fluid fills the gap, yet only fluid in the upper part of the gap is flowing. Velocity profiles through the gap are shown in Fig. 9, which have been taken along the line indicated by the arrow shown in Fig. 8. These profiles show very clearly the regions of sheared and unsheared fluid. Very similar behaviour has also been observed in bentonite–water suspensions.[29] These systems show intriguing similarities with the velocity profiles of wormlike micellar systems, which exhibit shear-banded flow in cone-and-plate.[20] Just as has been seen in shear-banded flow, there are regions of both low and high shear present in the gap.

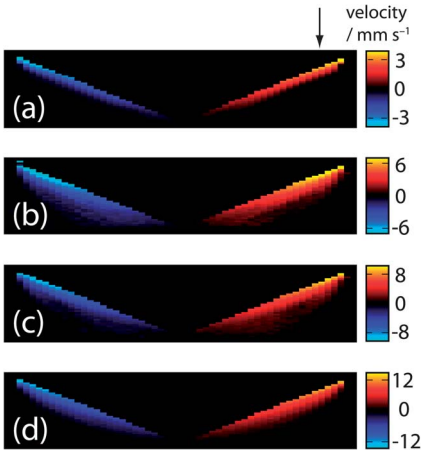

Fig. 8 Magnetic resonance velocity images for $[P_{6,6,6,14}][NTf_2]$ with 5% w/w Aerosil 200 in a cone-and-plate rheometer at rotation rates of (a) 0.08 Hz, (b) 0.16 Hz, (c) 0.23 Hz and (d) 0.32 Hz. The displayed field of view is 3.5 mm in the vertical direction and 20 mm in the horizontal direction, with a pixel size of 0.070 mm (vertical) × 0.313 mm (horizontal). The arrow indicates the position where velocity profiles were taken through the gap of the cone and plate in Fig. 9.

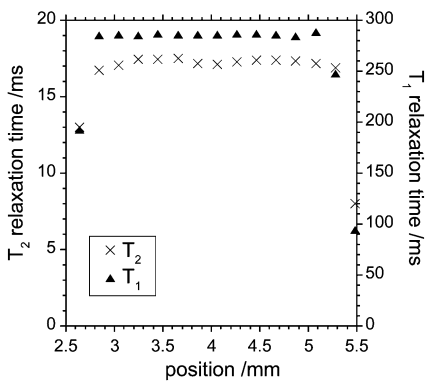

Fig. 7 Azimuthally averaged T_1 and T_2 magnetic resonance relaxation time profiles through the annulus of a Couette cell for $[P_{6,6,6,14}][NTf_2]$ with 5% w/w Aerosil 200 at $\omega = 1$ Hz.

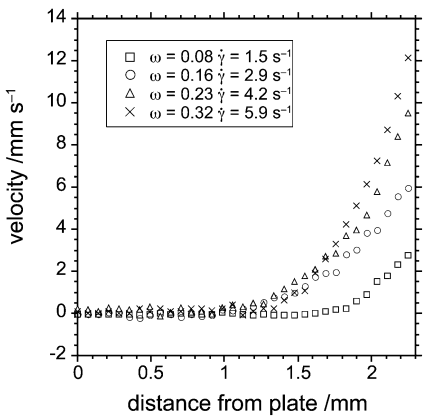

Fig. 9 Velocity profiles through the gap of a cone-and-plate rheometer for a suspension of $[P_{6,6,6,14}][NTf_2]$ + 5% w/w Aerosil 200, at a range of rotation rates, from the data shown in Fig. 8. Each profile was taken at a position of 6.56 mm from the tip of the cone, as indicated by the arrow in Fig. 8.

However, the structure of these regions is fundamentally different, with only two distinct shear regions present. While the composition of both wormlike micelle and colloidal systems are also rather different, what is similar is that both systems possess complex internal mesostructures, which will affect the flow properties of the system,[24] enabling shear-banding to occur. This is because, as flow affects the reorganisation of any internal structures, the reorganisation in turn affects the flow behaviour of the system and it is this coupling between internal mesostructure and flow that produces such nonlinear flow properties. Further work is needed to fully understand these issues.

Finally, our measurements have revealed different characteristic behaviour for the suspensions of hydrophilic silica in a hydrophobic or hydrophilic IL, which compare well with what have been previously observed for these and similar IL systems.[5,6,42] The hydrophilic $[C_4mim][BF_4]$ IL shows shear-thickening behaviour in both the conventional rheometric measurements, as well as the MR velocity imaging experiments. Interestingly, this marked increase in viscosity with shear rate, which has also been reported for $[C_2OHmim][NTf_2]$,[6] has not been widely reported for other ILs.[42] In both systems where it has been observed, it is believed that hydrogen bonding between the IL ($[BF_4^-]$ and $[C_2OHmim]$) and the silica were responsible for the observed rheology, by enabling a solvation layer to form around the silica particles.[5,6] A test for this hypothesis would be to monitor the mobility of these species under shear, and is planned for future work. In comparison to the $[C_4mim][BF_4]$ system, the hydrophobic $[P_{6,6,6,14}][NTf_2]$ IL shows shear-thinning behaviour, which has been observed in other hydrophobic ILs, such as $[C_2mim][NTf_2]$[6] and $[C_6mim][NTf_2]$.[42] However, our observations of the behaviour for the $[P_{6,6,6,14}][NTf_2]$ system in the MRI experiments raises some interesting questions about the behaviour of other IL suspensions exhibiting similar shear-thinning behaviour. While conventional rheometric measurements show shear-thinning behaviour, our MRI measurements of localised rheology show shear-banding behaviour. Hence, is the shear-banding behaviour observed in this phosphonium IL unique to this system or something that is common to other, or all, shear-thinning IL-silica suspensions? Further investigations are essential.

4 Conclusions

This paper reports the first investigation of the local rheology of ionic liquids in the presence and absence of dispersed silica nanoparticles using magnetic resonance velocity imaging. These measurements were combined with bulk rheological measurements. Two ionic liquids were investigated: $[C_4mim][BF_4]$ and $[P_{6,6,6,14}][NTf_2]$, which both demonstrated Newtonian behaviour when investigated in the absence of dispersed silica. However, more complex rheology was observed when hydrophilic silica was dispersed in either ionic liquid. In the bulk rheology measurements, the 15% w/w suspension of hydrophilic silica in $[C_4mim][BF_4]$ showed shear-thickening behaviour at higher shear rates (>10 s^{-1}). In the MR velocity measurements of this system in the Couette cell, a power law exponent of $n = 1$ (Newtonian behaviour) was observed at the lowest angular velocity studied, which increased to $n = 2.67$ (shear-thickening) at the highest angular velocity. These observations were in good agreement with those made by Ueno *et al.* on this system.[6] In addition to the investigation of $[C_4mim][BF_4]$ IL systems, this paper also reported the first rheological study of $[P_{6,6,6,14}][NTf_2]$. The $[P_{6,6,6,14}][NTf_2]$ + 5% silica system showed complex rheology and was found to exhibit shear-thinning behaviour, as well as the coexistence of regions of sheared and unsheared fluid when investigated using MR velocity imaging. The nature of this behaviour was investigated further, to test whether it could be explained as simply shear-localisation. However, closer inspection of the interface between the sheared and unsheared regions, as well as velocity images in a cone-and-plate rheometer suggested this was more likely to be shear-banding. We expect that the presence of this behaviour will have an impact on any bulk measurements of this system. In addition to this important observation, we believe that these velocity imaging experiments, particularly when combined with magnetic resonance relaxation measurements, have enormous potential in the investigation of the internal structure and molecular origins of the rheology of these complex systems.

Acknowledgements

The authors thank the University of Birmingham for support and the EPSRC and Royal Society for funding, Cytec and Evonik for the generous donation of the $[P_{6,6,6,14}][NTf_2]$ ionic liquid and Aerosil 200 respectively, and Nadine Barnard for the preparation of samples and rheometry measurements. JN thanks EPSRC for a PhD plus fellowship. The AR-G2 Rheometer (TA Instruments) used in this research was obtained through the Birmingham Science City: Innovative Uses for Advanced Materials in the Modern World (West Midlands Centre for Advanced Materials Project 2), with support from Advantage West Midlands (AWM) and part funded by the European Regional Development Fund (ERDF).

References

1 T. Welton, *Chem. Rev.*, 1999, **99**, 2071–2084.
2 D. R. MacFarlane, J. M. Pringle, P. C. Howlett and M. Forsyth, *Phys. Chem. Chem. Phys.*, 2010, **12**, 1659–1669.
3 I. Minami, *Molecules*, 2009, **14**, 2286–2305.
4 S. D. A. Lawes, S. V. Hainsworth, P. Blake, K. S. Ryder and A. P. Abbott, *Tribol. Lett.*, 2010, **37**, 103–110.
5 K. Ueno, K. Hata, T. Katakabe, M. Kondoh and M. Watanabe, *J. Phys. Chem. B*, 2008, **112**, 9013–9019.
6 K. Ueno, S. Imaizumi, K. Hata and M. Watanabe, *Langmuir*, 2009, **25**, 825–831.
7 K. Ueno and M. Watanabe, *Langmuir*, 2011, **27**, 9105–9115.
8 P. Wang, S. M. Zakeeruddin, P. Comte, I. Exnar and M. Gratzel, *J. Am. Chem. Soc.*, 2003, **125**, 1166–1167.
9 G. S. Fonseca, A. P. Umpierre, P. F. P. Fichtner, S. R. Teixeira and J. Dupont, *Chem.–Eur. J.*, 2003, **9**, 3263–3269.
10 J. Dupont, G. S. Fonseca, A. P. Umpierre, P. F. P. Fichtner and S. R. Teixeira, *J. Am. Chem. Soc.*, 2002, **124**, 4228–4229.

11 A. Gómez-Ramírez, M. T. López-López, F. González-Caballero and J. D. G. Durán, *Smart Mater. Struct.*, 2011, **20**, 045001.
12 C. Guerrero-Sanchez, T. Lara-Ceniceros, E. Jimenez-Regalado, M. Raşa and U. S. Schubert, *Adv. Mater.*, 2007, **19**, 1740–1747.
13 X. Cheng, J. H. McCoy, J. N. Israelachvili and I. Cohen, *Science*, 2011, **333**, 1276–1279.
14 G. S. Fonseca, G. Machado, S. R. Teixeira, G. H. Fecher, J. Morais, M. C. M. Alves and J. Dupont, *J. Colloid Interface Sci.*, 2006, **301**, 193–204.
15 L. S. Ott, M. L. Cline, M. Deetlefs, K. R. Seddon and R. G. Finke, *J. Am. Chem. Soc.*, 2005, **127**, 5758–5759.
16 K. Ueno, A. Inaba, M. Kondoh and M. Watanabe, *Langmuir*, 2008, **24**, 5253–5259.
17 G. L. Burrell, N. F. Dunlop and F. Separovic, *Soft Matter*, 2010, **6**, 2080–2086.
18 M. M. Britton and P. T. Callaghan, in *The Rheology of Lubricating Grease*, ed. C. Balan, ELGI, Amsterdam, 2000.
19 M. M. Britton, P. T. Callaghan, M. L. Kilfoil, R. W. Mair and K. M. Owens, *Appl. Magn. Reson.*, 1998, **15**, 287–301.
20 M. M. Britton and P. T. Callaghan, *Phys. Rev. Lett.*, 1997, **78**, 4930–4933.
21 M. M. Britton and P. T. Callaghan, *Magn. Reson. Chem.*, 1997, **35**, S37–S46.
22 G. Ovarlez, S. Rodts, X. Chateau and P. Coussot, *Rheol. Acta*, 2009, **48**, 831–844.
23 P. Callaghan, *Rheol. Acta*, 2008, **47**, 243–255.
24 S. M. Fielding, *Soft Matter*, 2007, **3**, 1262–1279.
25 S. Jarny, N. Roussel, S. Rodts, F. Bertrand, R. Le Roy and P. Coussot, *Cem. Concr. Res.*, 2005, **35**, 1873–1881.
26 A. Hess, M. Pretzl, L. Heymann, A. Fery and N. Aksel, *Phys. Rev. E: Stat., Nonlinear, Soft Matter Phys.*, 2011, **84**, 031407.
27 M. M. Britton and P. T. Callaghan, *J. Rheol.*, 1997, **41**, 1365–1386.
28 P. T. Callaghan and A. M. Gil, *Macromolecules*, 2000, **33**, 4116–4124.
29 P. Coussot, J. S. Raynaud, F. Bertrand, P. Moucheront, J. P. Guilbaud, H. T. Huynh, S. Jarny and D. Lesueur, *Phys. Rev. Lett.*, 2002, **88**, 218301.
30 M. M. Britton and P. T. Callaghan, *J. Texture Stud.*, 2000, **31**, 245–255.
31 P. T. Callaghan, *Translational dynamics and magnetic resonance*, OUP, Oxford, 2011.
32 P. T. Callaghan, *Principles of Nuclear Magnetic Resonance Microscopy*, Oxford University Press, Oxford, 1991.
33 M. M. Britton, *Chem. Soc. Rev.*, 2010, **39**, 4036–4043.
34 C. J. Rofe, R. K. Lambert and P. T. Callaghan, *J. Rheol.*, 1994, **38**, 875–887.
35 P. Coussot, L. Tocquer, C. Lanos and G. Ovarlez, *J. Non-Newtonian Fluid Mech.*, 2009, **158**, 85–90.
36 M. E. Cates, T. C. B. McLeish and G. Marrucci, *Europhys. Lett.*, 1993, **21**, 451–456.
37 H. Rehage and H. Hoffmann, *Mol. Phys.*, 1991, **74**, 933–973.
38 A. Cieniecka-Roslonkiewicz, J. Pernak, J. Kubis-Feder, A. Ramani, A. J. Robertson and K. R. Seddon, *Green Chem.*, 2005, **7**, 855–862.
39 A. Parmar, V. K. Aswal and P. Bahadur, *Spectrochim. Acta, Part A*, 2012, **97**, 137–143.
40 Magritek, *Prospa version 2.1*, http://www.magritek.com/prospa.html.
41 H. Yang, C. Z. Yu, Q. L. Song, Y. Y. Xia, F. Y. Li, Z. G. Chen, X. G. Li, T. Yi and C. H. Huang, *Chem. Mater.*, 2006, **18**, 5173–5177.
42 A. Wittmar, D. Ruiz-Abad and M. Ulbricht, *J. Nanopart. Res.*, 2012, **14**, 651.